Interfacial Engineering of Gallium Indium Phosphide Photoelectrodes for Hydrogen Evolution with Precious Metal and Non-Precious Metal Based Catalysts

Interfacial Engineering of Gallium Indium Phosphide Photoelectrodes for Hydrogen Evolution with Precious Metal and Non-Precious Metal Based Catalysts

Reuben J. Britto[†1]*, James L. Young*[†2]*, Ye Yang*[2]*, Myles A. Steiner*[3]*, David T. LaFehr*[2]*,*

Daniel J. Friedman[3]*, Mathew Beard*[2]*, Todd G. Deutsch*[2]*, Thomas F. Jaramillo*[1]*

[1]Department of Chemical Engineering, Shriram Center, Stanford University, 443 Via Ortega, Stanford, California 94305, United States

[2]Chemistry and Nanoscience Center, and Materials Science Center, National Renewable Energy Laboratory, Golden, Colorado 80401, United States

[3]National Center for Photovoltaics, National Renewable Energy Laboratory, Golden, Colorado 80401, United States

[†]These authors contributed equally to this work

AUTHOR INFORMATION

Corresponding Author

*Thomas F. Jaramillo. jaramillo@stanford.edu. Phone number: (650) 498 6879.

ABSTRACT

Gallium indium phosphide (GaInP$_2$) is a semiconductor with promising optical and electronic properties to serve as the large bandgap, top junction in a dual absorber tandem solar water splitting device. Poor intrinsic catalytic ability and surface corrosion in aqueous electrolyte remain key obstacles. Significant progress has been made developing thin-film protection layers and active catalysts for photoelectrochemical devices, but combining these into a catalytic protection layer that can provide long-term stability without sacrificing performance has proven difficult due, in large part, to challenges in developing active and stable interfaces. In this work, we demonstrate that a nanoscale molybdenum disulfide (MoS$_2$) film functions both as an effective protection layer and excellent hydrogen evolution catalyst for GaInP$_2$ photocathodes, with only a ~10% loss in initial light-limited current density after 100 h, and a photocurrent onset potential better than that of the same state-of-the-art device with a platinum-ruthenium catalyst. Using transient photoreflectance spectroscopy, we probed the carrier dynamics of these photocathodes and show that the MoS$_2$ coated device exhibits improved electron transfer at the surface interface compared to the PtRu catalyzed device. These MoS$_2$ protected devices are among the most active and stable single-absorber photocathodes for solar water splitting to date and offer a promising pathway towards generating hydrogen with high efficiency and significant longevity.

TOC GRAPHICS
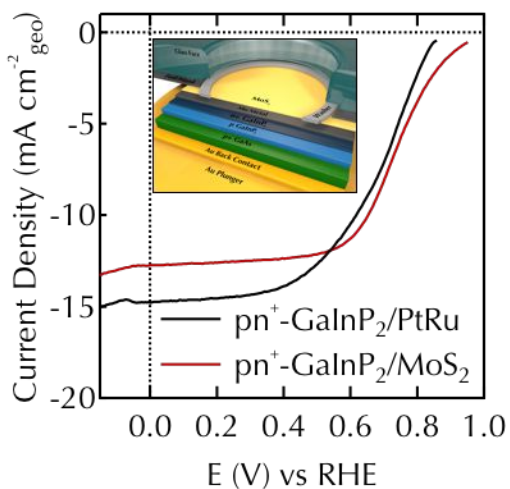
KEYWORDS

photoelectrochemisty, solar water splitting, hydrogen production, electrocatalysis, stability, III-V semiconductors.

TEXT

Hydrogen is a staple chemical in today's society. Millions of tonnes are utilized in processes ranging from oil refining, which produces 30% of the world's fuel, to ammonia production, which feeds 48% of humanity[1, 2, 3]. Currently, hydrogen is primarily produced from fossil fuels, but one pathway toward more sustainable production is to split water into hydrogen and oxygen using the energy from sunlight. Designing a device that can accomplish this efficiently and with long-term stability could have a major impact on today's industry by producing this commodity in a clean, economical fashion, with the possibility of growing its market as a primary energy carrier in place of fossil fuels[4].

Stability is a critical concern for many solar water splitting devices as semiconductors oftentimes undergo significant surface corrosion in the aqueous conditions required for efficient operation[5]. Substantial progress has been made extending the lifetime of semiconductors such as Si and GaAs with thin-film protection layers, such as titanium dioxide. However, to achieve high efficiency, these protection layers, which may be inert for the hydrogen or oxygen evolution reaction, often require the addition of a cocatalyst[5, 6]. Furthermore, while the energetics of the interfaces of these protection layers + cocatalysts have been studied experimentally and theoretically[7, 8, 9], further insight into the complex carrier dynamics of these systems is needed to understand and effectively engineer high performing devices.

In a dual-junction tandem absorber device, the protection + cocatalyst layers for the top absorber must be engineered to avoid significant light reflection and parasitic absorption. As a result, the devices with the greatest efficiencies use highly active precious metal cocatalysts, such as Pt and Rh, since they provide high turnover per active site and favorable HER onset potentials, limiting the loading needed and minimizing deleterious light blocking[10, 11, 12]. An earth-abundant thin-film material that can provide both long-term protection and efficient catalysis can eliminate the need for a separate protection layer and precious metal cocatalyst, reducing light blocking and cost.

Earth-abundant molybdenum sulfide nanomaterials possess excellent stability in acidic electrolyte and have edge sites with exceptional activity for the HER making them a superb candidate for a surface protection layer that has intrinsic catalytic ability[13, 14, 15].

Furthermore, recent studies have also demonstrated the effectiveness of MoS_2 as a protection layer on multiple semiconductors[15, 16, 17, 18]. Herein, we demonstrate that a thin coating of molybdenum disulfide can impart both long-term stability as well as effective catalytic ability to a pn^+-$GaInP_2$ photocathode. We further probe the $GaInP_2$ semiconductor interfacial carrier dynamics using transient photoreflectance spectroscopy (TPR) and highlight an important difference between conformal vs island catalysts in this system. $GaInP_2$ is a semiconductor with promising optical and electronic properties as the top absorber in a dual absorber tandem device but degrades within hours in the acidic conditions optimal for the hydrogen evolution reaction[17, 18, 19, 20, 21, 22]. In this work we show that after 100 h of testing, the MoS_2 protected device showed only a ~10% loss in light-limited current density, and the surface of the photocathode remained in pristine condition with no exposed $GaInP_2$ as measured using x-ray photoelectron spectroscopy (XPS). Furthermore, the MoS_2 protected device showed an improved onset potential of 0.91 V vs the reversible hydrogen electrode (RHE) compared to a similarly prepared pn^+-$GaInP_2$ photocathode coupled with a PtRu catalyst that exhibited an onset potential of 0.83 V vs RHE and which failed within only 6 hours of testing. Transient photoreflectance spectroscopy explains this improved onset by revealing improved electron transfer at the MoS_2-$GaInP_2$ interface compared to the PtRu-$GaInP_2$ interface.

This study, in concert with previous studies on Si and $GaInP_2$ photocathodes, demonstrates the promise of thin-films of MoS_2 as a non-precious protection layer whose activity is competitive with precious metal cocatalyzed devices in addition to exhibiting improved stability. These MoS_2 protected photocathodes are among the most active and

longest-lasting single junction devices to date and show promise to generate hydrogen with high efficiency and significant longevity. This will help enable the transition from lab-scale solar water splitting devices to prototype-scale devices that can generate meaningful quantities of hydrogen.

Photocathodic structure

Two different photocathode architectures were examined in this study and are illustrated in figures 1a and 1b. Both architectures use the same single crystal pn^+-GaInP$_2$ semiconductor epitaxially grown on a degenerately doped p-type GaAs substrate. The addition of ~25-nm thick n^+-GaInP$_2$ layer to a p-GaInP$_2$ photocathode provides ~0.5 V more positive photocurrent onset potential by improving band edge energy alignment at the electrolyte[23]. For the pn^+-GaInP$_2$/MoS$_2$ photocathode, the MoS$_2$ coating was synthesized by a partial thermal sulfidization of a sputtered thin film of Mo metal (see the Methods section). This method creates a thin, conformal surface coating of MoS$_2$ that provides an electronically conductive and protective barrier from the electrolyte, catalyzes the HER, and can be applied while minimizing parasitic light absorption[16, 17]. For the pn^+-GaInP$_2$/PtRu photocathode, PtRu nanoparticles were deposited onto a different part of the same pn^+-GaInP$_2$ wafer using flash sputtering in a manner identical to that of a 16.4%-efficient tandem III-V cell, one of the highest STH efficiencies for an integrated PEC device reported to date[10, 23]. This method was chosen to create a device that would be among the most active single junction photocathodes and represent a competitive comparison point for the pn^+-GaInP$_2$/MoS$_2$ photocathode.

To confirm successful fabrication of the desired architectures, cross-sectional scanning electron microscopy (SEM) was performed, as shown in figures 1c and 1d. The SEM images reveal the degenerately-doped GaAs epitaxial substrate and 1 um thick pn^+-GaInP$_2$ layer common to both architectures. The n+ layer is expected to be about 25 nm thick and have a doping density of about 7×10^{18} cm^{-3} (see Methods). For the pn^+-GaInP$_2$/MoS$_2$ photocathode, the synthesis of the Mo/MoS$_2$ layer is identical, except for a small temperature reduction in the sulfidization step, to one performed previously on a crystalline silicon substrate that was characterized with cross-sectional transmission electron microscopy (TEM)[16]. On the basis of these studies, the MoS$_2$ layer is expected to consist of several conformal stacked basal planes that reside on top of a thin layer of Mo metal. The total thickness of all the layers above the pn^+-GaInP$_2$ substrate is ~5 nm. For the pn^+-GaInP$_2$/PtRu photocathode, the deposition of the PtRu catalyst is identical to one performed previously on a tandem III-V cell that was characterized with STEM[23]. On the basis of this study, the PtRu is expected to consist of 2-5 nm particles with a surface coverage of about ~30%[23].

The composition and chemical state of the surface of both architectures were studied using XPS and are shown in figures 2 and 3. The pn^+-GaInP$_2$/MoS$_2$ photocathode shows peaks in the Mo 3d region and S 2p region. The peaks in the Mo 3d can be deconvoluted into 3 doublets indicating that Mo exists in 3 different states: a reduced metallic state consistent with Mo metal, a 4+ state consistent with MoS$_2$, and a 6+ state consistent with MoO$_3$[13, 24]. The S 2p region shows a peak corresponding to sulfur in the 2- state consistent with MoS$_2$[13, 24]. These XPS peaks are consistent with the Mo/MoS$_2$ layer

expected from TEM characterization of the MoS_2-Si system[16]. The absence of detectable peaks in the Ga 2p, In 3d, or P 2p regions further verifies the existence of a conformal Mo/MoS_2 layer on the surface of the pn^+-$GaInP_2$.

The pn^+-$GaInP_2$/PtRu photocathode shows peaks in Pt 4f, Ru 3p, Ga 2p, In 3d, and P 2p regions. The Pt 4f doublet is consistent with a reduced metallic Pt[25]. While the Ru 3p 1/2 peak is obfuscated by a Ga Auger peak, the Ru 3p 3/2 peak confirms that Ru also exists in a reduced metallic state[26, 27]. The Ga 2p and In 3d regions each show doublets of Ga and In in the 3+ oxidation state consistent with $GaInP_2$.[17, 27, 28] The P 2p region shows two doublets, one for P in the 3- oxidation state consistent with $GaInP_2$, and one for P in the 5+ oxidation state consistent with a metal phosphate[29, 30]. The presence of peaks in the Ga 2p, In 3d, and P 2p regions indicates that the PtRu catalyst does not form a conformal layer. This is consistent with the nanoparticulate conformation observed in the STEM characterization of the PtRu morphology on $GaInP_2$[23].

Electrochemical Performance

Following an established methodology[31], the PEC performance of the pn^+-$GaInP_2$/MoS_2 and pn^+-$GaInP_2$/PtRu photocathodes was evaluated in a three-electrode compression cell using 3M sulfuric acid electrolyte with 1 mM Triton X-100 (OmniTrace® EMD Millipore) surfactant added to expedite H_2 bubble evolution (additional details in Methods). The working electrodes were illuminated by a tungsten-halogen lamp with a water-filled IR filter and light shaping diffuser, and illumination intensity was set to "one sun" using a $GaInP_2$ reference cell calibrated to the AM1.5G standard[32]. The performance

of the photocathodes was first measured with a linear sweep voltammogram (LSV) scanning, under reverse bias, towards more positive potentials to determine the onset potential and light-limited photocurrent density. The voltammogram was halted when the current density reached about -0.5 mA cm^{-2} to prevent any surface oxidation from positive oxidative current. The LSV was immediately followed by a chronoamperometry (CA) measurement conducted at a constant potential of -0.3 vs. MSE (0.334 V vs. RHE). At this potential, the photocurrent is light limited, but the devices are still operating near the maximum power point. Such an operating point mimics the ideal operating point of a tandem device at short circuit, without excessive reverse bias that can inflate durability by increasing charge separation and cathodic protection while suppressing anodic corrosion mechanisms[23].

As shown in figure 4a, the pn$^+$-GaInP$_2$/MoS$_2$ photocathode demonstrated an onset potential of 0.91 V vs RHE at 1 mA cm^{-2}, while the pn$^+$-GaInP$_2$/PtRu demonstrated an onset potential of 0.83 V vs RHE. The light-limited current density attained by the pn$^+$-GaInP$_2$/MoS$_2$ photocathode was ~ 13 mA cm^{-2} while the pn$^+$-GaInP$_2$/PtRu photocathode achieved ~ 15 mA cm^{-2}. The pn$^+$-GaInP$_2$/MoS$_2$ photocathode was able to maintain its light-limited current density for 100 h without noticeable degradation, at which the point the experiment was terminated, and the sample was immediately transferred to a glove box and packaged air-free for post-analysis. The pn$^+$-GaInP$_2$/PtRu photocathode was able to maintain its light-limited current density for ~6 h at which point the device exhibited a sharp drop in current density indicating failure. (Figure 4b).

Catalytic onset

The onset potential is defined here as the potential at which the photocathode is able to begin catalyzing hydrogen production at an appreciable rate (i.e. 1 mA/cm^2). The pn$^+$-GaInP$_2$/MoS$_2$ and pn$^+$-GaInP$_2$/PtRu photocathodes demonstrated onsets that are among the best for a single absorber PEC device to date[5]. (Figure 4a, 6**)** This performance was anticipated for the pn$^+$-GaInP$_2$/PtRu photocathode given that it matches the paradigm common to the highest efficiency devices of a high quality III-V semiconductor coupled to a Pt-based catalyst[5, 10]. The more counterintuitive result is the ~80-mV improved onset potential for the pn$^+$-GaInP$_2$/MoS$_2$ photocathode since the intrinsic dark catalytic onset of MoS$_2$ for HER is known to be worse than that of PtRu[33, 34, 35, 36]. (Figure S1)

To help explain this result, transient photoreflectance (TPR) spectroscopy was used to probe the carrier dynamics at the surface of these photocathodes[9]. The prototypical TPR spectra for pn$^+$-GaInP$_2$, pn$^+$-GaInP$_2$/PtRu and pn$^+$-GaInP$_2$/MoS$_2$ are recorded at delay time of 5 ps and compared in Figure 5. All three spectra show sharp oscillatory peaks near the bandgap (1.8 eV), highlighted by the red shaded region. These spectral features suggest the presence of a strong surface electric field that causes oscillations in reflection spectra near the bandgap due to the Franz-Keldysh effect, and thus these oscillations are known as the Franz-Keldysh oscillations (FKO)[9]. After optical excitation, the separation of photocarriers driven by the surface field can partially screen the surface field, resulting in the oscillatory TPR spectra. In addition to these oscillatory features, a broad positive peak above the bandgap, near 1.96 eV, is present in the TPR spectra of pn$^+$-GaInP$_2$ and pn$^+$-GaInP$_2$/PtRu, indicated within the blue shaded regions. This broad band feature has

been attributed to the presence of electrons within the surface region of $GaInP_2$ through

the band filling effect and bandgap renormalization[9]. This feature is also present in the

TPR spectra for a related system, p-$GaInP_2$ (Figure S2), however this system exhibits a

shorter lifetime (<1ns) due to recombination and diffusion processes leading to

depopulation of surface carriers[37, 38]. The longer-lived photo-generated electrons at the

surface of pn^+-$GaInP_2$ and pn^+-$GaInP_2$/PtRu suggest lower surface recombination rates

and slower carrier diffusion into the bulk for GainP systems with a pn^+ junction.

Combined with the surface electric field evidenced by the FKO[9], we can conclude that

the electrons in pn^+-$GaInP_2$ and pn^+-$GaInP_2$/PtRu must be localized in a potential-well-

like energy band induced by band bending near the surface while the holes are spatially

separated from electrons (Figure 6). Interestingly, the same broad band feature near 1.96

eV is barely visible in the TPR spectra of pn^+-$GaInP_2$/MoS_2, even at short delay times,

implying the absence of the well-like band bending (Figure 6) which correlates to

improved electron transfer to MoS_2 at the interface.

As the TPR results indicate more efficient charge separation in pn^+-$GaInP_2$/MoS_2 relative

to pn^+-$GaInP_2$/PtRu, greater photovoltage would be expected in the pn^+-$GaInP_2$/MoS_2

system, which could explain the better photocurrent onset potential despite MoS_2 having

lower intrinsic catalytic activity than PtRu. We see that for this pn^+-$GaInP_2$

semiconductor system, a conformal catalyst layer is important, demonstrating a potential

advantage of continuous, 2D catalysts such as MoS_2 over metal catalysts, such as PtRu,

that do not readily wet surfaces as necessary to achieve continuous coverage. Poor

wetting characteristics require greater thickness for complete coverage, leading to

parasitic absorption/reflection losses by a metal catalyst. This finding may be relevant to other photoelectrodes with catalytic overlayers as there appears to be a fundamental and important dependence of performance on the catalyst conformality. This study only begins to reveal the complexity of this catalyst-semiconductor interface; we encourage additional investigations of various conformal and non-conformal catalysts fabricated with different semiconductors and characterized with photoelectrochemical methods (aqueous and non-aqueous) combined with advanced interface-focused techniques such as TPR.

Light-limited current density

The light-limited photocurrent density represents the yield of incident photons that are converted into current. Sufficiently thick $GaInP_2$ that has no reflection or recombination losses could achieve a maximum light-limited photocurrent density of ~19 mA cm^{-2} under AM1.5G illumination[17, 39]. Previous work done on a $GaInP_2$ PEC system has also established that Fresnel normal incidence reflectance can contribute to a 20-30% loss in maximum achievable external quantum efficiency[39]. The ~15 mA cm^{-2} (~18% STH) attained by the pn^+-$GaInP_2$/PtRu photocathode indicates that this device is subject to some reflective and parasitic absorptive losses[17, 40] (Figure 4a) which is expected given that no antireflective or light-trapping strategies were employed. Despite these losses, if paired with the proper photoanode, this photocathode could be the top absorber in an ~18% STH device. If an antireflective coating or other light trapping mechanism is used, an STH efficiency around ~20% could feasibly be achieved making this photocathode

attractive for inclusion in an unassisted tandem PEC device. The pn^+-GaInP$_2$/MoS$_2$ photocathode demonstrated a slightly smaller light-limited photocurrent of ~13 mA cm^{-2}, indicating that the Mo/MoS$_2$ layer may contribute to a greater amount of parasitic absorption (Figure 4a). This increased absorption is expected given the thicker and more conformal nature of the Mo/MoS$_2$ film. Previous absorption experiments on Mo/MoS$_2$ protected photocathodes have shown that the Mo/MoS$_2$ film can absorb as much as 40% of the incoming light across the spectrum[16, 17]. Even with this high parasitic absorption, pairing this photocathode with the right photoanode could create a device a ~16% STH efficiency. Future work will focus on improving the light-limited current density through strategies such as anti-reflective coatings, light-trapping mechanisms, and thinning of the protection layers.

Photocathode Stability

The pn^+-GaInP$_2$/MoS$_2$ photocathode demonstrated over 10x better stability than the pn^+-GaInP$_2$/PtRu photocathode (Figure 4b). The XPS spectra collected after the CA measurements, shown in figures 2 and 3, can explain why the pn^+-GaInP$_2$/PtRu photocathode failed catastrophically after 6 hours while the pn^+-GaInP$_2$/MoS$_2$ photocathode retained its activity after 100 hours. The pn^+-GaInP$_2$/PtRu photocathode, after testing, shows peaks in Pt4f, Ru 3p, Ga 2p, In 3d, P 2p and As 3p regions. The Pt 4f and Ru 3p doublets are consistent with a metallic PtRu catalyst indicating that the catalyst remains reduced on the surface[25, 26, 27]. The peaks in the Ga 2p region have gained shoulders and can be deconvoluted to show the formation of an oxide that likely formed from corrosive contact with the acidic electrolyte[27]. The In 3d and P 2p regions show

peaks relatively unchanged from spectra taken before testing, except for the appearance of As 3p peaks[41]. These peaks indicate that the $GaInP_2$ semiconductor layer corroded away so extensively as to expose the GaAs substrate underneath. The exposed GaAs substrate most likely created significant shunt and recombination pathways that contributed to the abrupt loss of light-limited photocurrent density[42].

The pn^+-$GaInP_2$/MoS_2 photocathode after testing only shows peaks in the Mo 3d and S 2p regions with no evidence of Ga, In, P, or As peaks. (Figure 3) In the Mo 3d region, the peaks can be deconvoluted into 2 doublets indicating that Mo exists in 2 different states: a reduced metallic state consistent with Mo metal and a 4+ state consistent with MoS_2[13, 24]. The peaks corresponding to Mo in the 6+ state consistent with MoO_3 are no longer present which is expected given that MoO_3 is unstable in sulfuric acid and dissolves[13]. The S 2p region shows a peak corresponding to sulfur in the 2- state consistent with MoS_2 and a new peak corresponding to S in the 6+ state consistent with SO_4^{2-}. This new peak is most likely due to residual sulfuric acid from the electrolyte[24]. The absence of peaks in the Ga 2p, In 3d, P 2p, and As 3p regions indicates that the substrate underneath the MoS_2 protection layer has not been exposed over the course of this test. The pn^+-$GaInP_2$/MoS_2 photocathode, after 100 hours of continuous operation in 3M sulfuric acid, appears to be in nearly pristine condition.

Comparing performance

When studying a photocathode for a dual-junction tandem absorber device, several important metrics for evaluating performance include the onset potential for the HER, the

light-limited current density, and the lifetime of the device. A better onset potential for a photocathode is a proxy for efficiency, and is critical because it relaxes the onset potential requirements for the photoanode, which involves the more sluggish kinetics of water oxidation, and/or allows the use of lower bandgaps for higher photocurrents and thus higher STH efficiency[20]. Light-limited current density and lifetime each provide useful information about a photocathode, with a key metric resulting from these two properties: the amount of hydrogen the photocathode can produce before failure. A high light-limited current density is not useful if the photocathode fails rapidly, and, conversely, a long lifetime is not valuable if the light-limited current density is too small—in both cases, very little hydrogen is produced. Multiplying these two properties together results in the combined metric of charge passed, a measurable value which directly correlates to total hydrogen produced.

Figure 7 compares the onset potential at 1 mA cm^{-2} vs RHE and the demonstrated charge passed for high-performing single absorber photocathodes with various thin-film protection schemes. This figure puts the different photocathodes that have been studied by researchers in this field in within context to help elucidate trends and useful insights for future device improvement. We see that crystalline silicon photocathodes are able to pass the largest amount of charge before failure but are unable to achieve high onset potentials even with precious metal catalysts. Conversely, III-V photocathodes tend to achieve high onset potentials but are unable to pass as much charge before failure. This trend is the basis for the strategy employed in this work: the charge passed by a pn$^+$-III-V photocathode could be improved by leveraging an MoS$_2$ protection scheme previously

shown to work on other systems[15, 16, 17]. Figure 7 also shows that most of the high performing devices, in terms of both onset potential and demonstrated charge passed, contain precious metal cocatalysts. The exception to this trend is the pn$^+$-GaInP$_2$/MoS$_2$ photocathode presented in this work. This photocathode used an earth-abundant cocatalyst, MoS$_2$, to achieve the highest reported onset potential for any single absorber III-V photocathode with or without precious metal catalysts. The MoS$_2$ thin-film also functioned as a very effective protection layer enabling the photocathode to also pass the most charge of any single absorber III-V photocathode reported to date.

As this MoS$_2$ protection scheme has been used successfully on semiconductors such as silicon and GaInP$_2$, this work further highlights the potential for MoS$_2$ nanomaterials to be used as catalytic thin-film protection schemes for many different water splitting semiconductors that are unstable in acid[15, 16, 17]. Successful stabilization of other III-V semiconductors could enable a multitude of highly efficient dual-absorber unassisted water splitting devices that can split water with high durability.

CONCLUSION

The pn$^+$-GaInP$_2$/MoS$_2$ device presented in this work is among the most active and stable single-absorber photocathodes for solar hydrogen production from water splitting. TPR spectral studies provided fundamental insights into the device's high performance, revealing that a conformal MoS$_2$ catalyst interface imparts improved electron transfer in addition to catalytic activity compared to a nonconformal PtRu catalyst. This insight on semiconductor-catalyst interfaces is potentially relevant to catalytically protected

photoectrodes across the field. As the pn^+-GaInP$_2$/MoS$_2$ photocathode presented in this work has a better onset and is significantly more stable than a sister pn^+-GaInP$_2$/PtRu photocathode, it demonstrates that a precious metal catalyst may not be a requirement for achieving high efficiencies in a photocathode. In fact, due to the substantial stability and interfacial properties it imparts, an MoS$_2$ catalytic protection layer may even be preferred. Future efforts to apply these MoS$_2$ protection layers to dual-junction tandem absorber devices offer the opportunity for highly efficient unassisted water splitting over long periods of time. These devices will enable sizeable quantities of hydrogen to be produced and help transition solar-water splitting from the lab-scale to the prototype-scale.

METHODS

Device Synthesis

The epitaxial GaInP$_2$ films were grown by ambient pressure organometallic vapor-phase epitaxy on degenerately Zn-doped GaAs(100) substrate pieces with 4° offcut toward (111)B. The substrates were precut to 20 mm x 30 mm and etched for 60 seconds in a dilute NH$_4$OH:H$_2$O$_2$:H$_2$O solution (1:2:10 by volume) before growth. A 1-µm thick Zn-doped GaInP$_2$ layer was grown first, with a nominal p-type carrier concentration of 10^{17} cm^{-3}. Then, the dopant was switched to Se to grow a 25-nm thick layer of n-type GaInP$_2$ with a nominal carrier concentration of $\sim 7x10^{18}$ cm^{-3}. [23] Following this, a 200 nm GaAs layer was grown and selectively etched off with an ammonium hydroxide (NH$_4$OH), hydrogen peroxide (H$_2$O$_2$), and water mixture (H$_2$O) in a 2:1:10 ratio. The GaAs contact layer was included to replicate the layer structures and post processing of inverted metamorphic multijunction devices (IMMs), the devices we plan to work on in the future[23]. After growth, Au ohmic contacts were electroplated to the back of the substrate.

MoS$_2$ deposition

The part of the wafer to be coated with MoS$_2$ was diced and transferred to a DC magnetron sputter coater. A thin layer of Mo metal was deposited onto the wafer at a rate of 7.2 nm min^{-1} for 30 seconds to achieve a nominal thickness of 3.6 nm. Immediately after Mo deposition, the wafer was transferred to a tube furnace and sulfidized in 90%H$_2$/10%H$_2$S held at 150 °C for 1 h to create the MoS$_2$ layer.

PtRu depostion

The PtRu was deposited via flash sputtering[23], in which the sample was passed briefly (< 1 s duration) underneath the sputter head to achieve very low PtRu loading (~500 ng/cm^2).

Physical and Chemical Characterization

X-ray photoelectron spectra of the pn$^+$-GaInP$_2$/PtRu and pn$^+$-GaInP$_2$/MoS$_2$ photocathodes before and after testing were collected using a Phi VersaPorbe Spectrometer with an Al Kalpha source. Binding energies were calibrated to the adventitious C 1s peak at 284.6 eV. SEM cross-sectional images were obtained using an FEI Magellan XHR microscope operated with the assistance of Pong Chakthranont. Cross-sectional images were taken instead of surface images because both samples appeared as blank gray surfaces since the Mo/MoS$_2$ layer is flat and conformal and the PtRu nanoparticles were too small to readily resolve by SEM.

Electrochemical Characterization

To make photoelectrodes, the sample was cleaved into about 7 mm x 7 mm pieces, with the MoSx- and PtRu-modified sample edges trimmed off to prevent the possibility of shorting. The PEC characterization and durability testing were performed in a compression cell described elsewhere[31] that facilitated the post-durability analyses. The electrolyte was 3M H_2SO_4 with 1 mM Triton X-100 (both OmniTrace® EMD Millipore) surfactant added. The Pt foil (Premion® 99.997%) counter electrode (1 cm x 2.5 cm) was housed in a glass tube with medium-porosity glass frit end that was filled with the same electrolyte but without surfactant to mitigate counter electrode fouling and solution yellowing (same reference). A Koslow Scientific Co. mercury/mercurous sulfate (Hg/Hg_2SO_4) reference electrode (MSE) with 3M H_2SO_4 filling solution was used (reference potential of 0.634 V vs. normal hydrogen electrode). Illumination was provided by a 250 W quart tungsten halogen lamp with water-filled IR filter and light-shaping diffuser (Newport). The illumination intensity was set to match the AM1.5G calibration current of a 1.81 eV bandgap $GaInP_2$ reference cell. Current-voltage measurements were taken at a 20 mV/s scan rate from negative to positive potential while blocking/unblocking the light source at 0.1 V intervals twice to simultaneously measure the dark current. The scan would begin in the light limited current density region and the electrolyte in the vicinity of the working electrode would rapidly saturate with H_2 while scanning towards the onset potential. Durability testing was performed at constant potential of -0.3 V vs MSE (0.334 vs RHE) while monitoring photocurrent density. For post-analysis, the

19

compression cell was transferred to an Ar-filled glove box immediately after stopping the durability test, where the sample was removed from the cell, rinsed with DI water, dried with Ar, and vacuum packaged in Ar. After characterization with XPS, no additional chronoamperometry or voltammetry was performed since the characterization process (rinsing, pumping cycles, etc.) can accelerate failure.

Transient Photoreflectance Characterization

Femtosecond TPR spectroscopy is based on a regeneratively amplified Ti:sapphire laser system. The 800nm output beam is ~4 mJ per pulse with 1 kHz repetition rate. The pump for TPR is generated by doubling the frequency of the fundamental pulses (~1.5 mJ/pulse) in a BBO crystal, and it is then chopped at a frequency of 500 Hz. The pump power is attenuated by neutral density filter wheels. The broadband probe pulses (420-830 nm) are generated by focusing 800nm beam into a sapphire crystal. The probe pulses are delayed in time with respect to the pump pulses using a motorized translation stage. The pump and probe are spatially overlapped on the surface of the sample, and the reflected probe pulses are directed to the multichannel CMOS sensors by optical cables. The beam spot diameters on the sample for probe and pump are 250 μm and 1.4 mm, respectively. The total pump photon flux is determined by measuring the pump power after a pinhole with radius of 200 μm at the sample position. The

input photon flux is obtained by subtracting the reflected photon flux from the total photon flux. The carrier density is calculated as the ratio of input photon flux to the penetration depth that is 1 over absorption coefficient at the excitation photon energy.

ASSOCIATED CONTENT

Supporting Information.

Additional details on the dark catalytic performance and the transient photoreflectance measurement.

AUTHOR INFORMATION

Corresponding Author

*E-mail: jaramillo@stanford.edu. Phone: (650) 498 6879

Notes

The authors declare no competing financial interests.

FIGURES

Figure 1. Photocathode device structures. Schematic of a fully synthesized a) pn$^+$-GaInP$_2$/PtRu and b) pn$^+$-GaInP$_2$/MoS$_2$ photocathode being tested in a compression cell. Cross-sectional SEM images of the surface region of c) pn$^+$-GaInP$_2$/PtRu and d) pn$^+$-GaInP$_2$/MoS$_2$ photocathode.
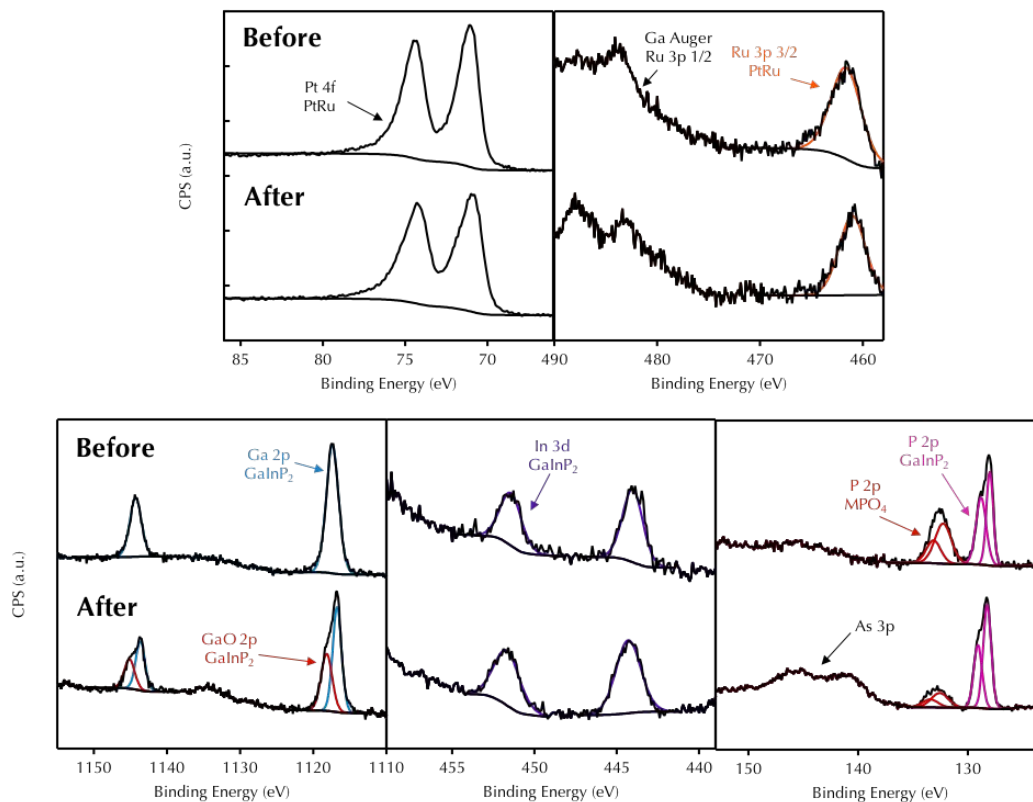
Figure 2. XPS measurements of a pn$^+$-GaInP$_2$/PtRu photocathode before and after electrochemical LSV and CA testing. Before testing, the surface of the device consists of Pt and Ru in a reduced metallic state, Ga and In in the 3+ oxidation state consistent with GaInP$_2$, and P in a 3- oxidation state corresponding to GaInP$_2$, and a 5+ oxidation state corresponding to a metal phosphate. After testing, a Ga surface oxide has grown, and the underlying GaAs substrate has been exposed due to the appearance of an As 3p peak.
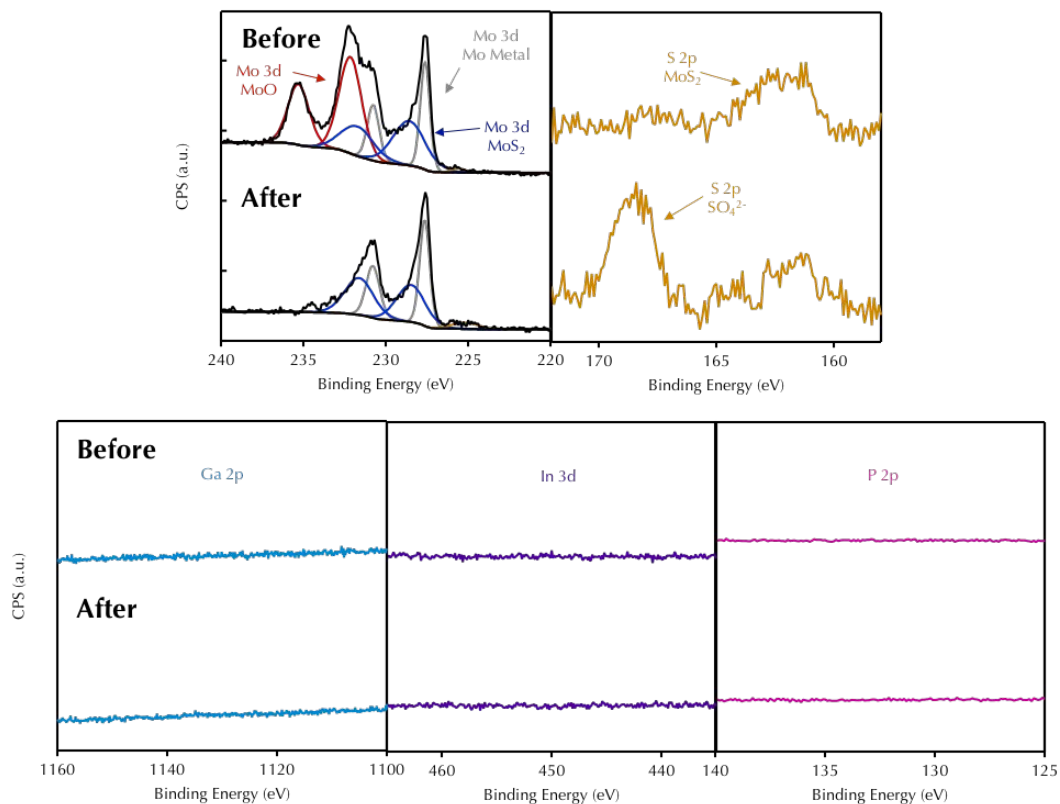
Figure 3. XPS measurements of a pn$^+$-GaInP$_2$/MoS$_2$ photocathode before and after electrochemical LSV and CA testing. Before testing, the surface of the device consists of Mo in a reduced metallic state consistent with Mo metal, a 4+ state consistent with MoS$_2$, and a 6+ state consistent with MoO$_3$ and S in a 2- state consistent with MoS$_2$. After testing, the only change is the absence of peaks corresponding to Mo in a 6+ state corresponding to MoO$_3$, indicating that the surface remains relatively pristine.
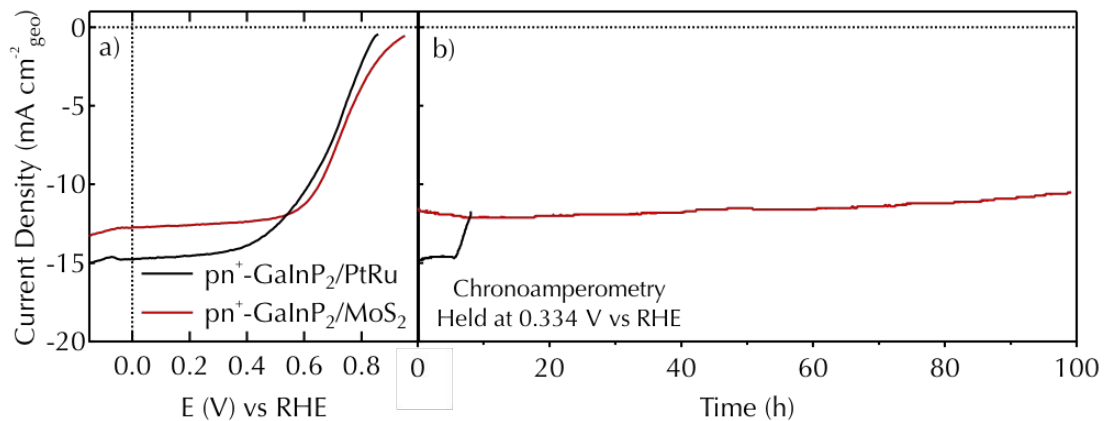
Figure 4. Electrochemical characterization of the pn+-GaInP$_2$/PtRu and pn+-GaInP$_2$/MoS$_2$ photocathodes in 3M sulfuric acid. a) LSV collected prior to stability testing b) CA measurement taken at a constant potential of 0.334 V vs RHE.
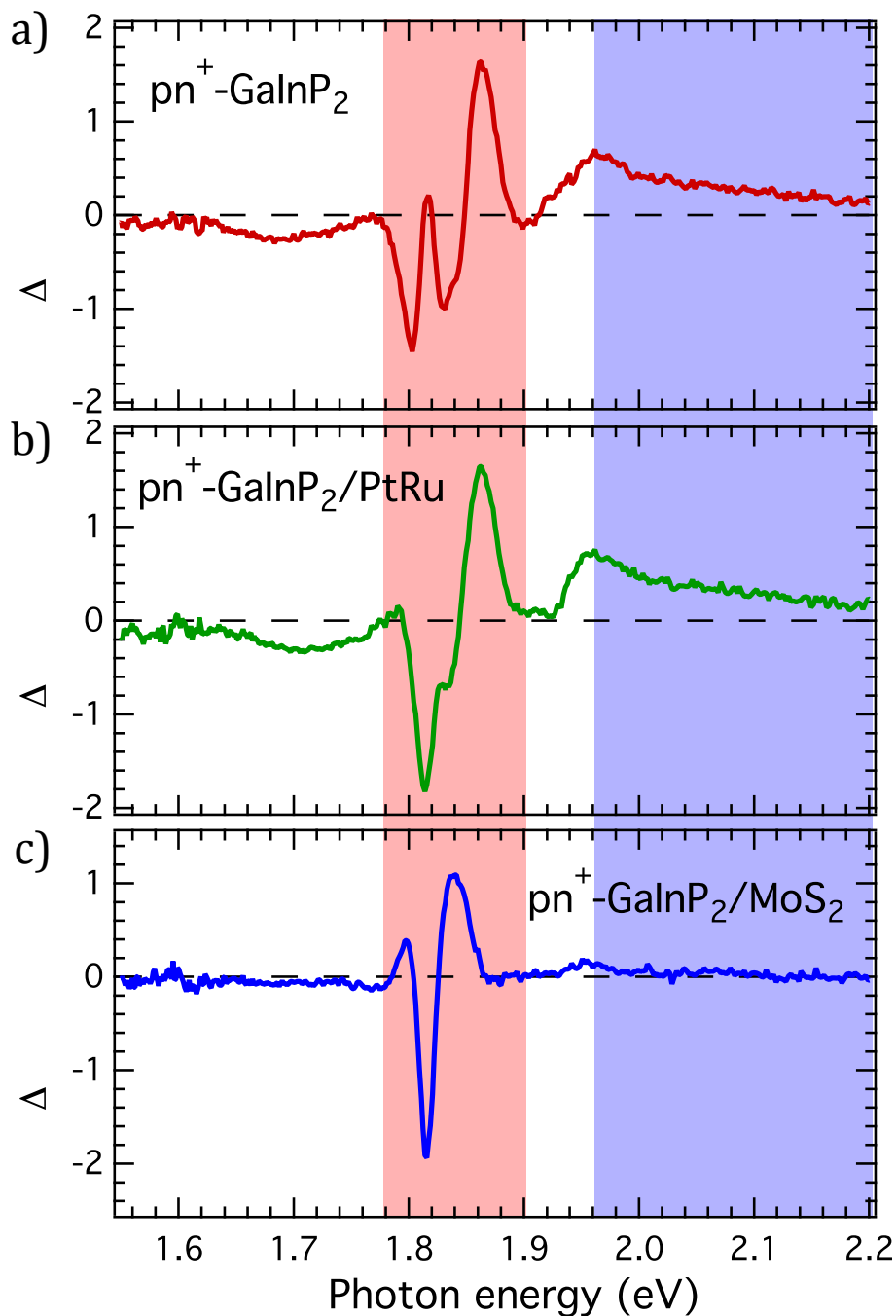
Figure 5. TPR spectra of the samples. These TPR spectra are recorded at 5 ps delay time. The y-axis and x-axis represent the photo-induced reflection change and probe photon energy. The red and blue shade areas indicate the FKO and surface electron induced reflection change, respectively.
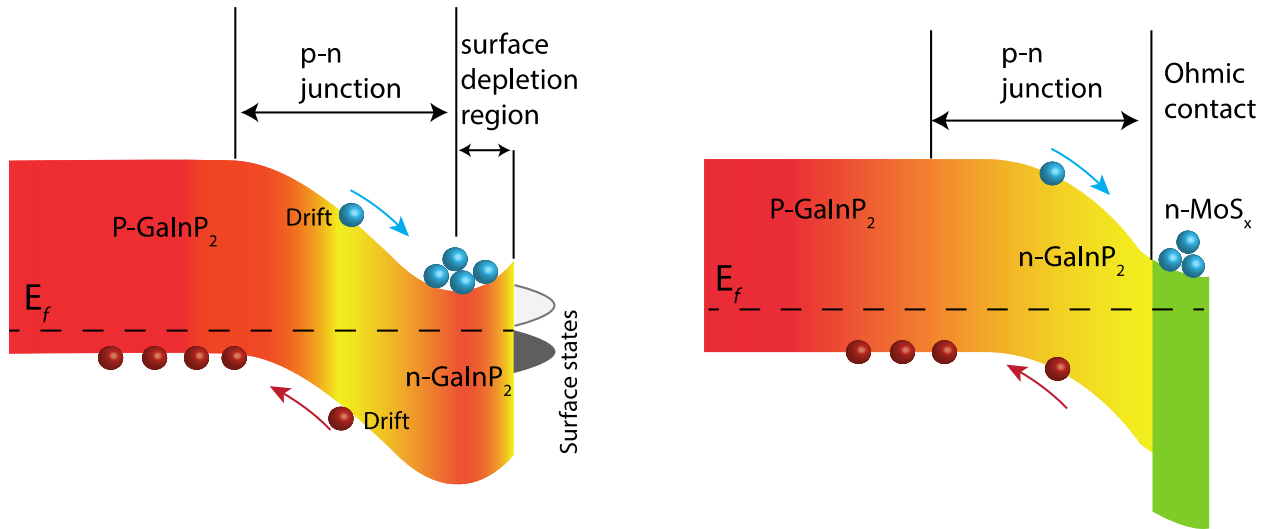
Figure 6. Illustrations of the proposed energy bands for pn$^+$-GaInP$_2$ and pn$^+$-GaInP$_2$/MoS$_2$. For pn$^+$-GaInP$_2$, the surface electric field bends the band up near the surface, leading to an energy valley that traps electrons. For pn$^+$-GaInP$_2$/MoS$_2$, the n-MoS$_2$ contact removes the surface states of n-GaInP$_2$ and avoids forming the energy valley, and thus the photo-generated electrons in GaInP$_2$ are quickly injected into the MoS$_2$ layer.
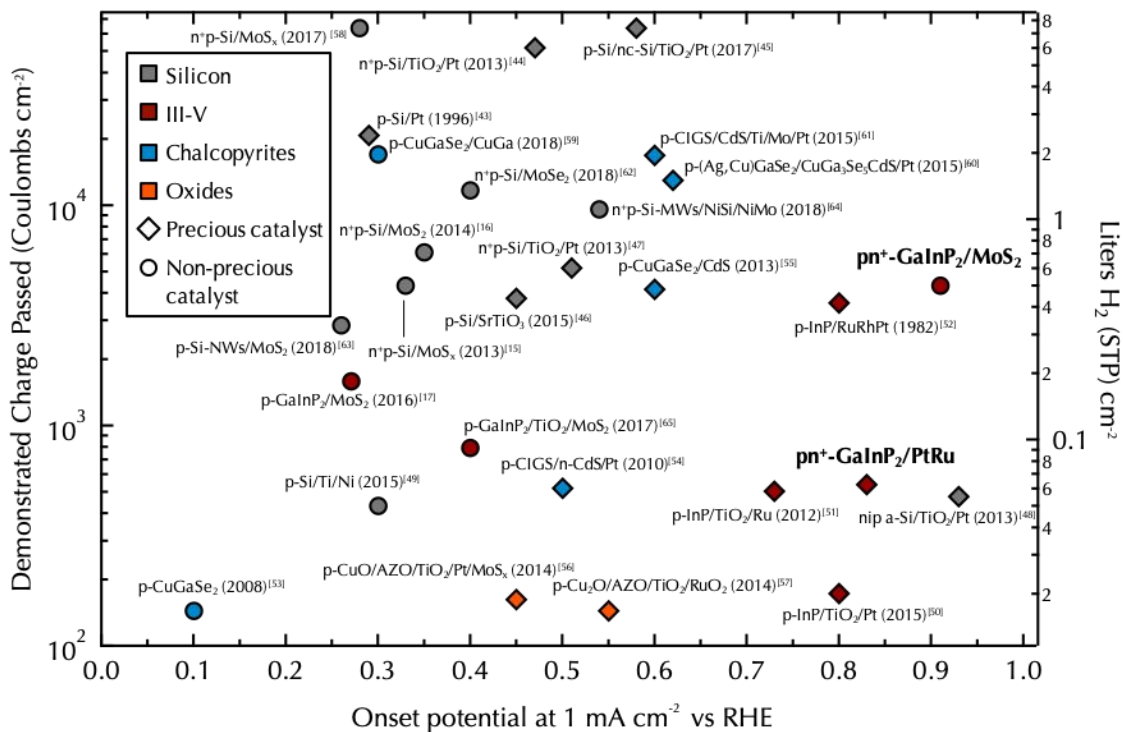
Figure 7. Comparison of the onset potential at 1 mA cm^{-2} vs RHE and the demonstrated charge passed for high-performing single absorber photocathodes with various thin-film protection schemes. The photocathodes with the highest reported activities and stabilities using silicon, III-V, chalcopyrite, and oxide light absorbers were included and delineated by the use of precious and non-precious metal cocatalysts. The pn$^+$-GaInP$_2$/PtRu and pn$^+$-GaInP$_2$/MoS$_2$ photocathodes (labeled in bold) are from this work. The demonstrated charge passed was calculated by combining the reported light-limited current density and the reported stability. The liters of H$_2$ at STP was calculated assuming 100% faradaic yield for hydrogen production from the light limited current density. The tabulated data

from this figure can be found in the supplementary information in Table S1.[15,16, 17, 43, 44, 45, 46, 47, 48, 49, 50, 51, 52, 53, 54, 55, 56, 57, 58,59,60,61,62,63,64,65]

REFERENCES

1.   US Department of Energy: Quadrennial Technology Review; 2015.

2.   International Energy Agency *Key World Energy Statistics*; 2016.

3.   Erisman JW, Sutton MA, Galloway J, Klimont Z, Winiwarter W. How a century of ammonia synthesis changed the world. *Nature Geosci* 2008, **1**(10)**:** 636-639.

4.   Bard AJ, Fox MA. Artificial Photosynthesis: Solar Splitting of Water to Hydrogen and Oxygen. *Acc Chem Res* 1995, **28**(3)**:** 141-145.

5.   Hu S, Lewis NS, Ager JW, Yang J, McKone JR, Strandwitz NC. Thin-Film Materials for the Protection of Semiconducting Photoelectrodes in Solar-Fuel Generators. *J Phys Chem C* 2015, **119**(43)**:** 24201-24228.

6.   Gu J, Yan Y, Young JL, Steirer KX, Neale NR, Turner JA. Water reduction by a p-GaInP2 photoelectrode stabilized by an amorphous TiO2 coating and a molecular cobalt catalyst. *Nat Mater* 2016, **15**(4)**:** 456-460.

7.   Rossi RC, Lewis NS. Investigation of the Size-Scaling Behavior of Spatially Nonuniform Barrier Height Contacts to Semiconductor Surfaces Using Ordered Nanometer-Scale Nickel Arrays on Silicon Electrodes. *The Journal of Physical Chemistry B* 2001, **105**(49)**:** 12303-12318.

8.   Pham TA, Ping Y, Galli G. Modelling heterogeneous interfaces for solar water splitting. *Nat Mater* 2017, **16**(4)**:** 401-408.

9.   Yang Y, Gu J, Young JL, Miller EM, Turner JA, Neale NR*, et al.* Semiconductor interfacial carrier dynamics via photoinduced electric fields. *Science* 2015, **350**(6264)**:** 1061.

10.   Ager JW, Shaner MR, Walczak KA, Sharp ID, Ardo S. Experimental demonstrations of spontaneous, solar-driven photoelectrochemical water splitting. *Energy Environ Sci* 2015, **8**(10)**:** 2811-2824.

11.   Trotochaud L, Mills TJ, Boettcher SW. An Optocatalytic Model for Semiconductor–Catalyst Water-Splitting Photoelectrodes Based on In Situ Optical Measurements on Operational Catalysts. *J Phys Chem Lett* 2013, **4**(6)**:** 931-935.

12.   May MM, Lewerenz H-J, Lackner D, Dimroth F, Hannappel T. Efficient direct solar-to-hydrogen conversion by in situ interface transformation of a tandem structure. *Nature Communications* 2015, **6:** 8286.

13.   Chen Z, Cummins D, Reinecke BN, Clark E, Sunkara MK, Jaramillo TF. Core–shell MoO3–MoS2 Nanowires for Hydrogen Evolution: A Functional Design for Electrocatalytic Materials. *Nano Lett* 2011, **11**(10)**:** 4168-4175.

14.   Keong Koh EW, Chiu CH, Lim YK, Zhang Y-W, Pan H. Hydrogen adsorption on and diffusion through MoS2 monolayer: First-principles study. *Int J Hydrogen Energy* 2012, **37**(19)**:** 14323-14328.

15.   Laursen AB, Pedersen T, Malacrida P, Seger B, Hansen O, Vesborg PCK*, et al.* MoS2—an integrated protective and active layer on n+p-Si for solar H2 evolution. *PCCP* 2013, **15**(46)**:** 20000-20004.

16.   Benck JD, Lee SC, Fong KD, Kibsgaard J, Sinclair R, Jaramillo TF. Designing Active and Stable Silicon Photocathodes for Solar Hydrogen Production Using Molybdenum Sulfide Nanomaterials. *Adv Energy Mater* 2014, **4**(18)**:** 1-8.

17.   Britto RJ, Benck JD, Young JL, Hahn C, Deutsch TG, Jaramillo TF. Molybdenum Disulfide as a Protection Layer and Catalyst for Gallium Indium Phosphide Solar Water Splitting Photocathodes. *J Phys Chem Lett* 2016, **7**(11)**:** 2044-2049.

18.   Gu J, Aguiar JA, Ferrere S, Steirer KX, Yan Y, Xiao C*, et al.* A graded catalytic–protective layer for an efficient and stable water-splitting photocathode. *Nature Energy* 2017, **2:** 16192.

19.   Pinaud BA, Benck JD, Seitz LC, Forman AJ, Chen Z, Deutsch TG*, et al.* Technical and economic feasibility of centralized facilities for solar hydrogen production via photocatalysis and photoelectrochemistry. *Energy Environ Sci* 2013, **6**(7)**:** 1983-2002.

20.   Doscher H, Geisz JF, Deutsch TG, Turner JA. Sunlight absorption in water - efficiency and design implications for photoelectrochemical devices. *Energy Environ Sci* 2014, **7**(9)**:** 2951-2956.

21.   Khaselev O, Turner JA. A Monolithic Photovoltaic-Photoelectrochemical Device for Hydrogen Production via Water Splitting. *Science* 1998, **280**(5362)**:** 425-427.

22.   Khaselev O, Turner JA. Electrochemical Stability of p‐GaInP2 in Aqueous Electrolytes Toward Photoelectrochemical Water Splitting. *J Electrochem Soc* 1998, **145**(10)**:** 3335-3339.

23.   Young JL, Steiner MA, Döscher H, France RM, Turner JA, Deutsch Todd G. Direct solar-to-hydrogen conversion via inverted metamorphic multi-junction semiconductor architectures. *Nature Energy* 2017, **2:** 17028.

24.   Nielsen JH, Bech L, Nielsen K, Tison Y, Jørgensen KP, Bonde JL, *et al.* Combined spectroscopy and microscopy of supported MoS2 nanoparticles. *Surf Sci* 2009, **603**(9)**:** 1182-1189.

25.   Dückers K, Bonzel HP, Wesner DA. Surface core level shifts of Pt(111) measured with Y Mχ radiation (132.3 eV). *Surf Sci* 1986, **166**(1)**:** 141-158.

26.   Shen JY, Adnot A, Kaliaguine S. An ESCA study of the interaction of oxygen with the surface of ruthenium. *Appl Surf Sci* 1991, **51**(1)**:** 47-60.

27.   Cossu G, Ingo GM, Mattogno G, Padeletti G, Proietti GM. XPS investigation on vacuum thermal desorption of UV/ozone treated GaAs(100) surfaces. *Appl Surf Sci* 1992, **56–58, Part 1:** 81-88.

28.   Faur M, Faur M, Jayne DT, Goradia M, Goradia C. XPS investigation of anodic oxides grown on p-type InP. *Surf Interface Anal* 1990, **15**(11)**:** 641-650.

29.   Sundararaman CS, Lafontaine H, Poulin S, Mouton A, Currie JF. Reactive sputtering of InP in N2 and N2/O2 plasmas. *J Vac Sci Technol B* 1991, **9**(3)**:** 1433-1439.

30.   Streubel P, Peisert H, Hesse R, Chassé T, Szargan R. Chemical bonding studies on UV/ozone- and (NH4)2S-treated InP(001) surfaces by x-ray photoelectron spectroscopy and x-ray induced Auger electron spectroscopy. *Surf Interface Anal* 1995, **23**(9)**:** 581-588.

31.   Young JL, Steirer KX, Dzara MJ, Turner JA, Deutsch TG. Remarkable stability of unmodified GaAs photocathodes during hydrogen evolution in acidic electrolyte. *Journal of Materials Chemistry A* 2016, **4**(8)**:** 2831-2836.

32.   Standard Tables for Reference Solar Spectral Irradiances: Direct Normal and Hemispherical on 37° Tilted Surface. ASTM Interational; 2012.

33.   Benck JD, Hellstern TR, Kibsgaard J, Chakthranont P, Jaramillo TF. Catalyzing the Hydrogen Evolution Reaction (HER) with Molybdenum Sulfide Nanomaterials. *ACS Catalysis* 2014, **4**(11)**:** 3957-3971.

34.   Jaramillo TF, Jørgensen KP, Bonde J, Nielsen JH, Horch S, Chorkendorff I. Identification of Active Edge Sites for Electrochemical H2 Evolution from MoS2 Nanocatalysts. *Science* 2007, **317**(5834)**:** 100-102.

35.   Greeley J, Jaramillo TF, Bonde J, Chorkendorff I, Norskov JK. Computational high-throughput screening of electrocatalytic materials for hydrogen evolution. *Nat Mater* 2006, **5**(11)**:** 909-913.

36. Greeley J, Nørskov JK, Kibler LA, El-Aziz AM, Kolb DM. Hydrogen Evolution Over Bimetallic Systems: Understanding the Trends. *ChemPhysChem* 2006, **7**(5)**:** 1032-1035.

37. Yang Y, Yang M, Moore David T, Yan Y, Miller Elisa M, Zhu K*, et al.* Top and bottom surfaces limit carrier lifetime in lead iodide perovskite films. *Nature Energy* 2017, **2:** 16207.

38. Yang Y, Yan Y, Yang M, Choi S, Zhu K, Luther JM*, et al.* Low surface recombination velocity in solution-grown CH3NH3PbBr3 perovskite single crystal. *Nature Communications* 2015, **6:** 7961.

39. Doscher H, Young JL, Geisz JF, Turner JA, Deutsch TG. Solar-to-hydrogen efficiency: shining light on photoelectrochemical device performance. *Energy Environ Sci* 2016, **9**(1)**:** 74-80.

40. Schubert M, Gottschalch V, Herzinger CM, Yao H, Snyder PG, Woollam JA. Optical constants of GaxIn1−xP lattice matched to GaAs. *J Appl Phys* 1995, **77**(7)**:** 3416-3419.

41. DeLouise LA. Investigation of the mechanism of Ar+ ion-assisted Cl2 etching of GaAs{110}: Role of ion-induced charge acceptor states. *J Appl Phys* 1991, **70**(3)**:** 1718-1729.

42. Benghanem MS, Alamri SN. Modeling of photovoltaic module and experimental determination of serial resistance. *Journal of Taibah University for Science* 2009, **2:** 94-105.

43. Maier CU, Specht M, Bilger G. Hydrogen evolution on platinum-coated p-silicon photocathodes. *Int J Hydrogen Energy* 1996, **21**(10)**:** 859-864.

44. Seger B, Tilley DS, Pedersen T, Vesborg PCK, Hansen O, Gratzel M*, et al.* Silicon protected with atomic layer deposited TiO2: durability studies of photocathodic H2 evolution. *RSC Advances* 2013, **3**(48)**:** 25902-25907.

45. Bae D, Pedersen T, Seger B, Iandolo B, Hansen O, Vesborg PCK*, et al.* Carrier-selective p- and n-contacts for efficient and stable photocatalytic water reduction. *Catal Today* 2017, **290:** 59-64.

46. Ji L, McDaniel MD, Wang S, Posadas AB, Li X, Huang H*, et al.* A silicon-based photocathode for water reduction with an epitaxial SrTiO3 protection layer and a nanostructured catalyst. *Nat Nano* 2015, **10**(1)**:** 84-90.

47. Seger B, Pedersen T, Laursen AB, Vesborg PCK, Hansen O, Chorkendorff I. Using TiO2 as a Conductive Protective Layer for Photocathodic H2 Evolution. *JACS* 2013, **135**(3)**:** 1057-1064.

48.   Lin Y, Battaglia C, Boccard M, Hettick M, Yu Z, Ballif C, *et al.* Amorphous Si Thin Film Based Photocathodes with High Photovoltage for Efficient Hydrogen Production. *Nano Lett* 2013, **13**(11)**:** 5615-5618.

49.   Feng J, Gong M, Kenney MJ, Wu JZ, Zhang B, Li Y, *et al.* Nickel-coated silicon photocathode for water splitting in alkaline electrolytes. *Nano Research* 2015, **8**(5)**:** 1577-1583.

50.   Lin Y, Kapadia R, Yang J, Zheng M, Chen K, Hettick M, *et al.* Role of TiO2 Surface Passivation on Improving the Performance of p-InP Photocathodes. *J Phys Chem C* 2015, **119**(5)**:** 2308-2313.

51.   Lee MH, Takei K, Zhang J, Kapadia R, Zheng M, Chen Y-Z, *et al.* p-Type InP Nanopillar Photocathodes for Efficient Solar-Driven Hydrogen Production. *Angew Chem Int Ed* 2012, **51**(43)**:** 10760-10764.

52.   Heller A, Aharon-Shalom E, Bonner W, Miller B. Hydrogen-evolving semiconductor photocathodes: nature of the junction and function of the platinum group metal catalyst. *JACS* 1982, **104**(25)**:** 6942-6948.

53.   Marsen B, Cole B, Miller EL. Photoelectrolysis of water using thin copper gallium diselenide electrodes. *Sol Energy Mater Sol Cells* 2008, **92**(9)**:** 1054-1058.

54.   Yokoyama D, Minegishi T, Maeda K, Katayama M, Kubota J, Yamada A, *et al.* Photoelectrochemical water splitting using a Cu(In,Ga)Se2 thin film. *Electrochem Commun* 2010, **12**(6)**:** 851-853.

55.   Moriya M, Minegishi T, Kumagai H, Katayama M, Kubota J, Domen K. Stable Hydrogen Evolution from CdS-Modified CuGaSe2 Photoelectrode under Visible-Light Irradiation. *JACS* 2013, **135**(10)**:** 3733-3735.

56.   Morales-Guio CG, Tilley SD, Vrubel H, Grätzel M, Hu X. Hydrogen evolution from a copper(I) oxide photocathode coated with an amorphous molybdenum sulphide catalyst. *Nature Communications* 2014, **5:** 3059.

57.   Tilley SD, Schreier M, Azevedo J, Stefik M, Graetzel M. Ruthenium Oxide Hydrogen Evolution Catalysis on Composite Cuprous Oxide Water-Splitting Photocathodes. *Adv Funct Mater* 2014, **24**(3)**:** 303-311.

58.   King LA, Hellstern TR, Park J, Sinclair R, and Jaramillo TF. Highly Stable Molybdenum Disulfide Protected Silicon Photocathodes for Photoelectrochemical Water Splitting. *ACS Applied Materials & Interfaces* 2017, **9**(42): 36792-36798.

59. Muzzillo CP, Klein WE, Li Z, DeAngelis AD, Horsley K, Zhu K, and Gaillard N. Low-Cost, Efficient and Durable H2 Production by Photoelectrochemical Water Splitting with CuGa$_3$Se$_5$ Photocathodes. *ACS Applied Materials & Interfaces* Just Accepted Manuscript

60. Zhang L, Minegishi T, Nakabayashi M, Suzuki Y, Seki K, Shibata N, Kubota J, Domen K. Durable Hydrogen Evolution from Water Driven by Sunlight Using (Ag,Cu)GaSe2 Photocathodes Modified with Cds and CuGa3Se5. *Chemical Science* 2015, **6**, 894-901.

61. Kumagai H, Minegishi T, Sato N, Yamada T, Kubota J, Domen K. Efficient Solar Hydrogen Production from Neutral Electrolytes Using Surface-Modified Cu(in,Ga)Se2 Photocathodes. Journal of Materials Chemistry A 2015, **3**, 8300-8307.

62. Huang, G.; Mao, J.; Fan, R.; Yin, Z.; Wu, X.; Jie, J.; Kang, Z.; Shen, M. Integrated Mose2 with N+P-Si Photocathodes for Solar Water Splitting with High Efficiency and Stability. Appl. Phys. Lett. 2018, 112, 013902.

63. Hu, D.; Xiang, J.; Zhou, Q.; Su, S.; Zhang, Z.; Wang, X.; Jin, M.; Nian, L.; Nozel, R.; Zhou, G.; et al. One-Step Chemical Vapor Deposition of Mos2 Nanosheets on Sinws as Photocathodes for Efficient and Stable Solar-Driven Hydrogen Production. Nanoscale 2018, 10, 3518-3525.

64. Wouter Vijselaar, Roald M. Tiggelaar, Han Gardeniers, and Jurriaan Huskens. Efficient and Stable Silicon Microwire Photocathodes with a Nickel Silicide Interlayer for Operation in Strongly Alkaline Solutions Wouter Vijselaar, Roald M. Tiggelaar, Han Gardeniers, and Jurriaan Huskens ACS Energy Letters 2018 3 (5), 1086-1092.

65. Gu, J.; Aguiar, J. A.; Ferrere, S.; Steirer, K. X.; Yan, Y.; Xiao, C.; Young, James L.; Al-Jassim, M.; Neale, N. R.; Turner, J. A. A Graded Catalytic– Protective Layer for an Efficient and Stable Water-Splitting Photocathode. Nature Energy 2017, 2, 16192.